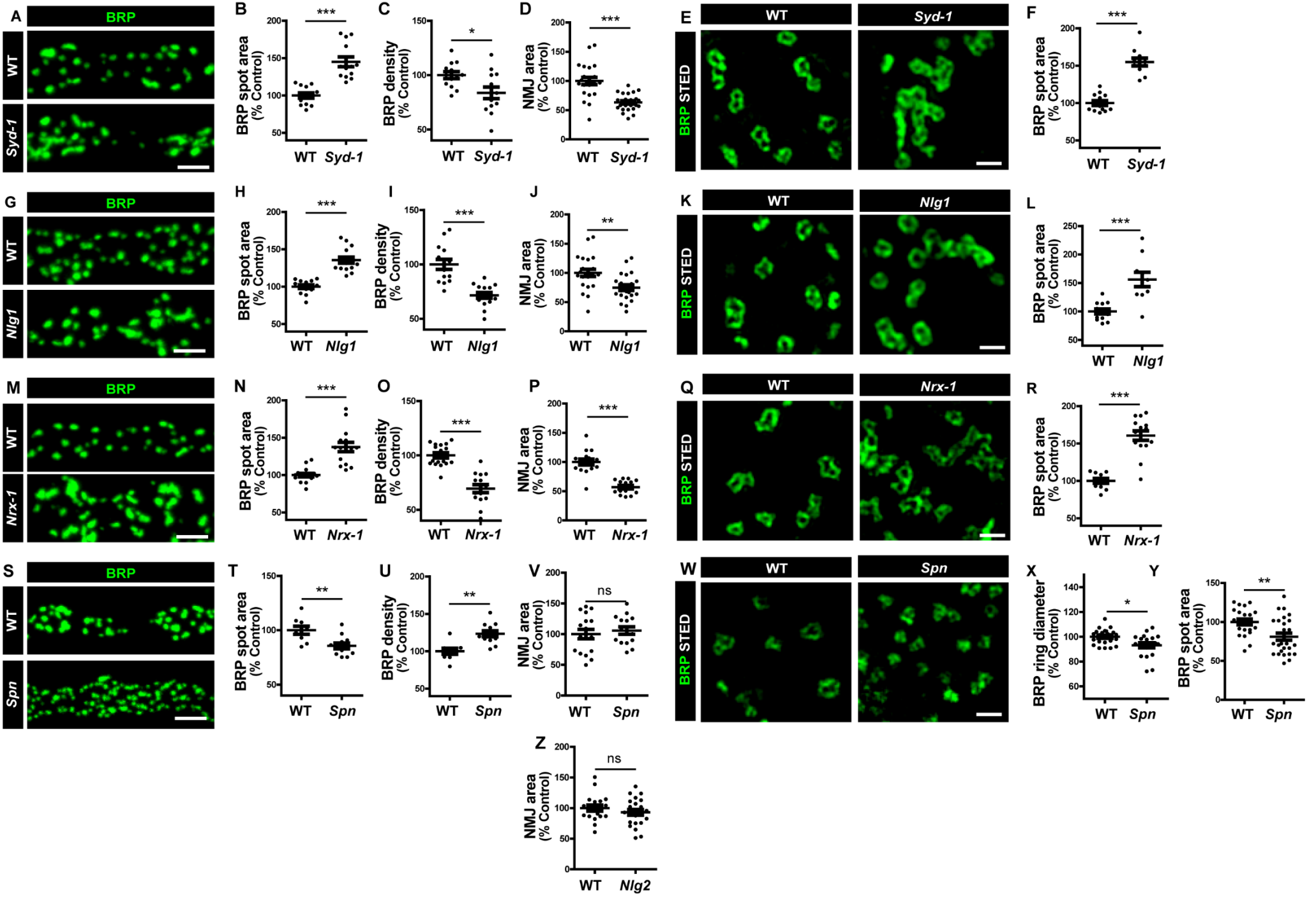
A
BRP
WT
Syd-1
B
BRP spot area (% Control)
***
WT
Syd-1
C
BRP density (% Control)
*
WT
Syd-1
D
NMJ area (% Control)
***
WT
Syd-1
E
WT
Syd-1
BRP STED
F
BRP spot area (% Control)
***
WT
Syd-1
G
BRP
WT
Nlg1
H
BRP spot area (% Control)
***
WT
Nlg1
I
BRP density (% Control)
***
WT
Nlg1
J
NMJ area (% Control)
**
WT
Nlg1
K
WT
Nlg1
BRP STED
L
BRP spot area (% Control)
***
WT
Nlg1
M
BRP
WT
Nrx-1
N
BRP spot area (% Control)
***
WT
Nrx-1
O
BRP density (% Control)
***
WT
Nrx-1
P
NMJ area (% Control)
***
WT
Nrx-1
Q
WT
Nrx-1
BRP STED
R
BRP spot area (% Control)
***
WT
Nrx-1
S
BRP
WT
Spn
T
BRP spot area (% Control)
**
WT
Spn
U
BRP density (% Control)
**
WT
Spn
V
NMJ area (% Control)
ns
WT
Spn
W
WT
Spn
BRP STED
X
BRP ring diameter (% Control)
*
WT
Spn
Y
BRP spot area (% Control)
**
WT
Spn
Z
NMJ area (% Control)
ns
WT
Nlg2

Figure S1. *Syd-1, Nlg1* and *Nrx-1* mutant phenotypes are similar. *Spn* and *Nlg2* mutant phenotypes are similar. Related to figures 1 and 2.

(A,G,M,S) Representative images of 3rd instar larval muscle 4 NMJs immunostained with an antibody against BRP. Scale bars: 2µm. (A-D) *Syd-1*, (G-J) *Nlg1* and (M-P) *Nrx*-1 mutants show sparse, overgrown AZs and smaller NMJ areas. (S-U) *Spn* mutants show supernumerary, smaller AZs. (V,Z) *Spn* and *Nlg2* mutants show no change in NMJ areas. (E,K,Q,W) BRP scaffolds resolved through STED microscopy show (E-F) *Syd-1,* (K-L) *Nlg1* and (Q-R) *Nrx*-1 mutants show large, clumsy BRP scaffolds while (W-Y) *Spn* mutants show smaller BRP scaffolds compared to controls.

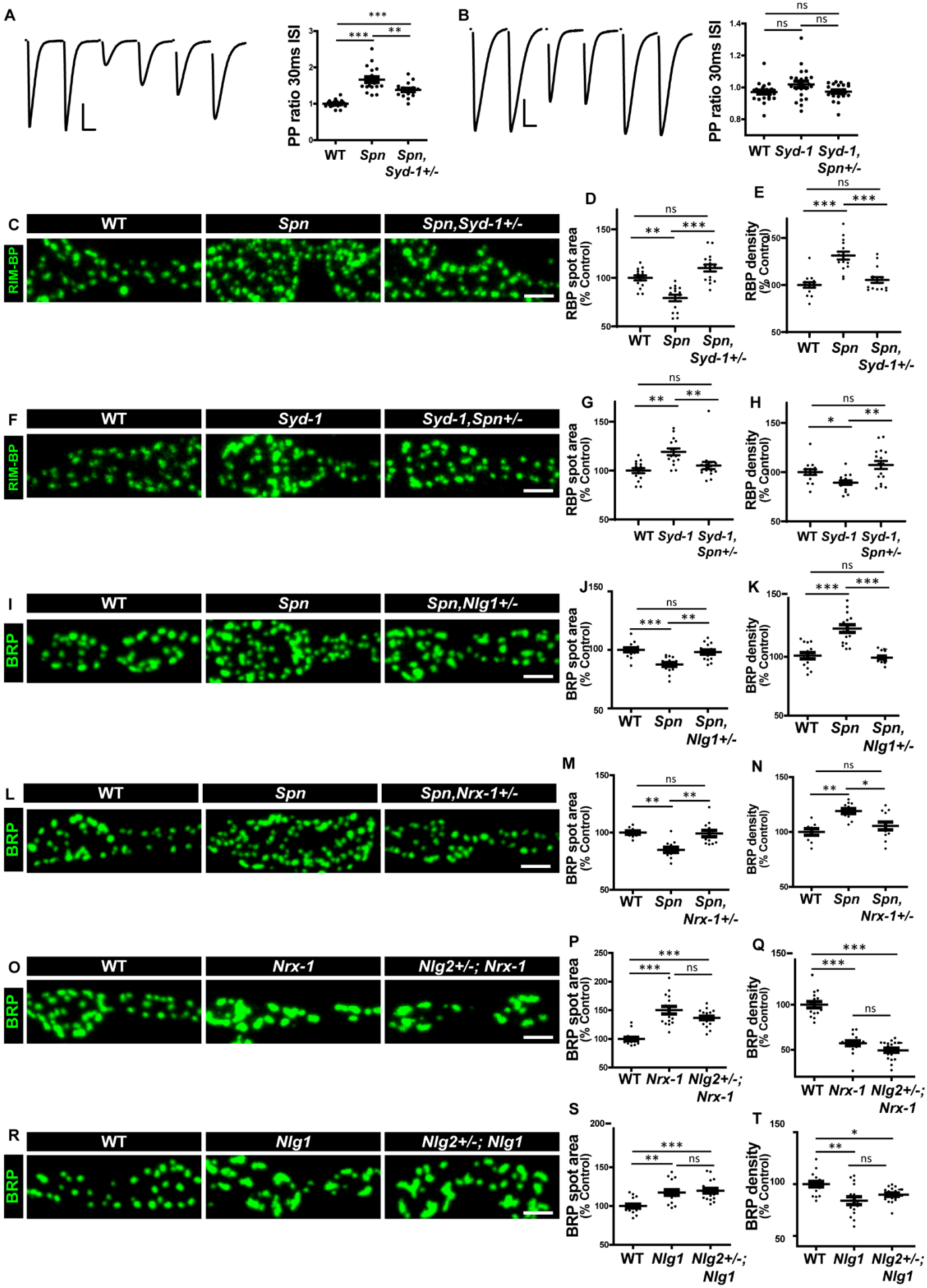
A
PP ratio 30ms ISI
WT
Spn
Spn, Syd-1+/-
B
PP ratio 30ms ISI
WT
Syd-1
Syd-1, Spn+/-
C
WT
Spn
Spn,Syd-1+/-
RIM-BP
D
RBP spot area (% Control)
E
RBP density (% Control)
F
WT
Syd-1
Syd-1,Spn+/-
RIM-BP
G
RBP spot area (% Control)
H
RBP density (% Control)
I
WT
Spn
Spn,Nlg1+/-
BRP
J
BRP spot area (% Control)
K
BRP density (% Control)
L
WT
Spn
Spn,Nrx-1+/-
BRP
M
BRP spot area (% Control)
N
BRP density (% Control)
O
WT
Nrx-1
Nlg2+/-; Nrx-1
BRP
P
BRP spot area (% Control)
Q
BRP density (% Control)
R
WT
Nlg1
Nlg2+/-; Nlg1
BRP
S
BRP spot area (% Control)
T
BRP density (% Control)

Figure S2. Syd-1/Nlg1 and Spn/Nlg2 take on antagonistic trans-synaptic signalling roles in presynapse development. Related to figures 1 and 2.

(A,B) Representative traces of paired-pulse (inter stimulus interval (ISI) of 30ms) measurements at muscle 6/7 NMJs. Scale bars: 10ms, 20mV. (A) Increased paired pulse ratio (30ms PPI) of *Spn* mutants is rescued by *Syd-1* heterozygosity. (B) Paired pulse ratio (30ms PPI) is unchanged in *Syd-1* mutants. (C-R) Representative images of 3rd instar larval muscle 4 NMJs immunostained with antibodies against RIM-BP or BRP. Scale bars: 2µm. Quantification of RIM-BP spot area and density show that *Spn* and *Syd-1* mutant phenotypes are rescued by (C-E) *Syd-1* and (F-H) *Spn* heterozygosity, respectively. Quantification of BRP spot area density show that *Spn* mutant phenotype is suppressed by (I-K) *Nlg1* and (L-M) *Nrx-1* heterozygosity. (O-Q) *Nrx-1* and (R-T) *Nlg1* mutant phenotypes are suppressed by *Nlg2* heterozygosity.

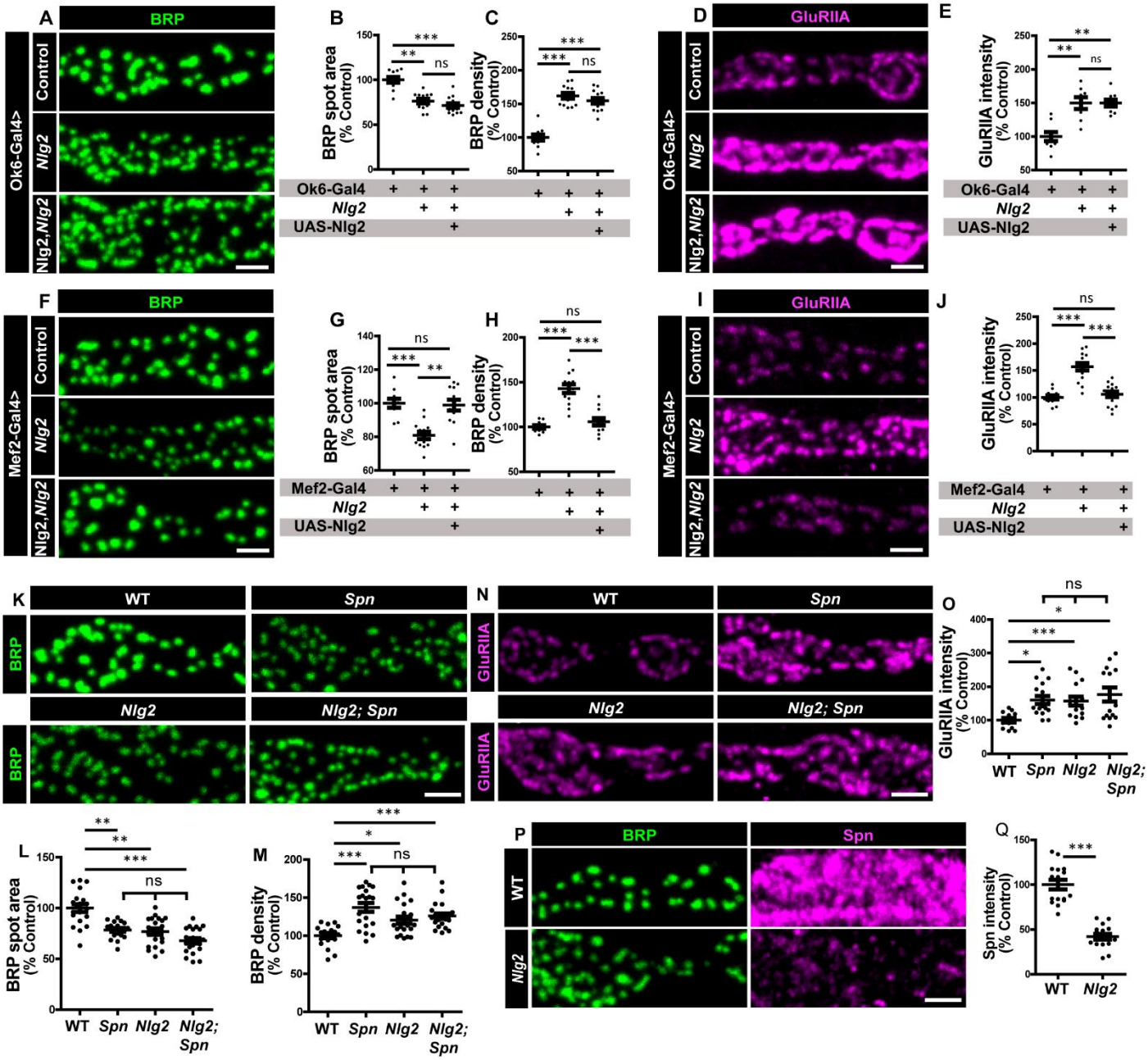

Figure S3. *Nlg2* phenotype is rescued by transgenic expression of Nlg2 in the postsynaptic muscle cell. Related to figure 2.

Representative images of 3rd instar larval muscle 4 NMJs immunostained with antibodies against BRP (green) and, (A-N) GluRIIA (magenta) or (P) Spn (magenta). Scale bars: 2µm. Quantification of BRP spot area and density, and GluRIIA intensity, show that *Nlg2* mutant phenotype is rescued by reexpression of Nlg2 in the (F-J) muscle, but not in the (A-E) motoneuron. (K-O) Double mutants of *Spn* and *Nlg2* are non-additive in their BRP and GluRIIA phenotypes. (P-Q) *Nlg2* mutants show lower levels of Spn.

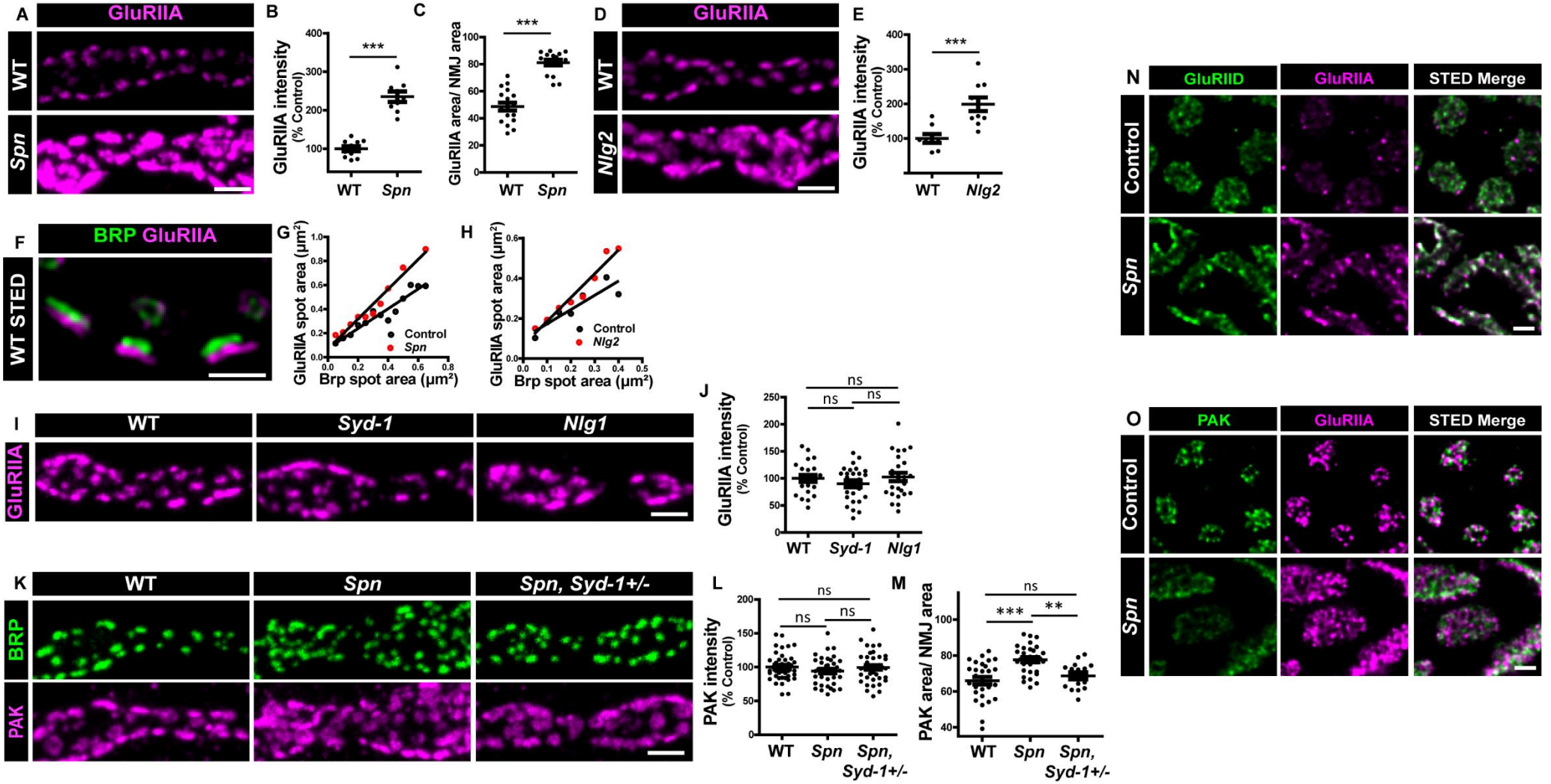

Figure S4. *Syd-1, Nlg1* and *Nrx-1* mutant phenotypes are similar. *Spn* and *Nlg2* mutant phenotypes are similar. Excessive GluRIIA in *Spn* mutants is part of the PSD. Related to figure 3.

(A,D,I) Representative images of 3rd instar larval muscle 4 NMJs immunostained with antibodies against GluRIIA. Scale bars: 2µm. (A-B) *Spn* and (D-E) *Nlg2* mutants show higher levels of GluRIIA. (C) Quantification of the ratio of GluRIIA receptor field area to NMJ area shows overgrown receptor fields in *Spn* mutants. (F) STED microscopy of BRP and GluRIIA show pre- and post-synapse matching. Scale bar: 500nm.

(G,H) Linear regression lines fit to BRP spot area plotted against GluRIIA field area show that *Spn* and *Nlg2* mutants accumulate excessive GluRIIA opposite BRP scaffolds. (I) *Syd-1* and *Nlg1* mutants accumulate GluRIIA to wildtype levels. (K) Representative images of NMJs immunostained with antibodies against BRP (green) and PAK (magenta). Scale bars: 2µm. (L) PAK intensity is unchanged in *Spn* mutants, but (M) the area of NMJ covered by PAK increases in *Spn* mutants, suppressed by *Syd-1* heterozygosity. (N) GluRIIA and GluRIID, which form a complex in vivo colocalize in WT and *Spn* mutants. (O) GluRIIA and PAK also colocalize in WT and *Spn* mutants. Scale bar: 500nm.

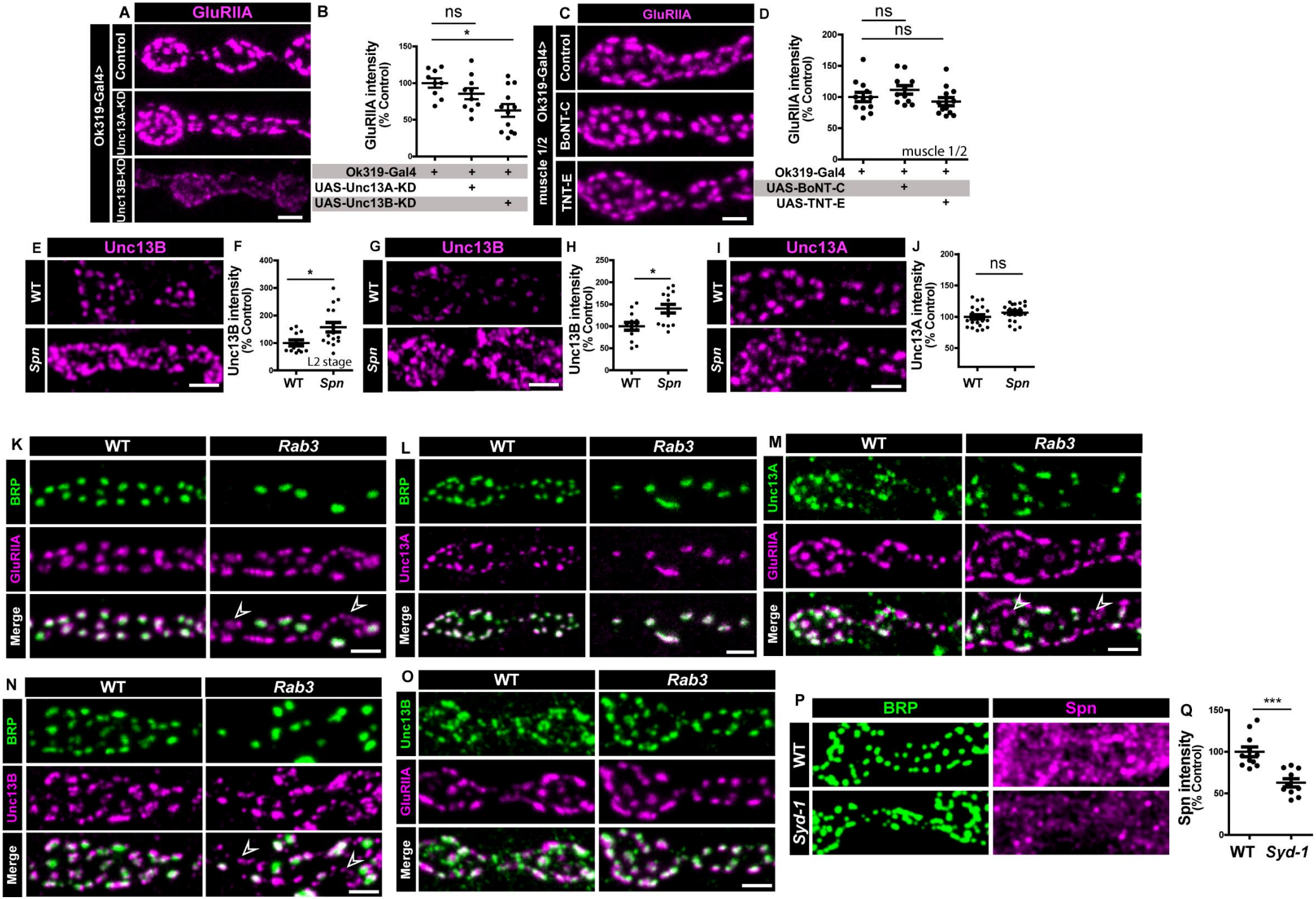
A
GluRIIA
Ok319-Gal4>
Control
Unc13A-KD
Unc13B-KD
B
ns
*
GluRIIA intensity (% Control)
Ok319-Gal4
UAS-Unc13A-KD
UAS-Unc13B-KD
C
GluRIIA
muscle 1/2
Ok319-Gal4>
Control
BoNT-C
TNT-E
D
ns
ns
GluRIIA intensity (% Control)
muscle 1/2
Ok319-Gal4
UAS-BoNT-C
UAS-TNT-E
E
Unc13B
WT
Spn
F
*
Unc13B intensity (% Control)
L2 stage
WT
Spn
G
Unc13B
WT
Spn
H
*
Unc13B intensity (% Control)
WT
Spn
I
Unc13A
WT
Spn
J
ns
Unc13A intensity (% Control)
WT
Spn
K
WT
Rab3
BRP
GluRIIA
Merge
L
WT
Rab3
BRP
Unc13A
Merge
M
WT
Rab3
Unc13A
GluRIIA
Merge
N
WT
Rab3
BRP
Unc13B
Merge
O
WT
Rab3
Unc13B
GluRIIA
Merge
P
BRP
Spn
WT
Syd-1
Q
***
Spn intensity (% Control)
WT
Syd-1

Figure S5. Spn mutants have higher Unc13B protein levels. Unc13B facilitates GluRIIA incorporation in absence of Unc13A. *Syd-1* mutants show lower levels of Spn. Related to figures 4 and 5.

(A-P) Representative images of NMJs immunostained with antibodies as mentioned in the figure. Scale bars: 2µm. (A-B) Motoneuronal KD of *Unc13B* impairs GluRIIA accumulation, but KD of Unc13A has no effect. (C-D) Ok319-Gal4 driving UAS-BoNT-C and UAS-TNT-E shows no change in GluRIIA intensity in muscles 1/2. (E-J) *Spn* mutants show elevated Unc13B levels in both L2 and L3 larval developmental stages, while Unc13A levels remain unchanged. (K) BRP and GluRIIA accumulate in half the available synapses in *Rab3* mutants; GluRIIA also accumulates in the other half unopposed by BRP. (L) Unc13A colocalizes with BRP (M) Not all GluRIIA fields are apposed by Unc13A in *Rab3.* (N) Unc13B accumulates in spots negative for BRP in *Rab3*. (O) All GluRIIA fields are apposed by Unc13B in both *Rab3* mutants and controls. (P-Q) Quantification of Spn intensity in *Syd-1* mutants shows that *Syd-1* mutants accumulate Spn to lower levels compared to controls.

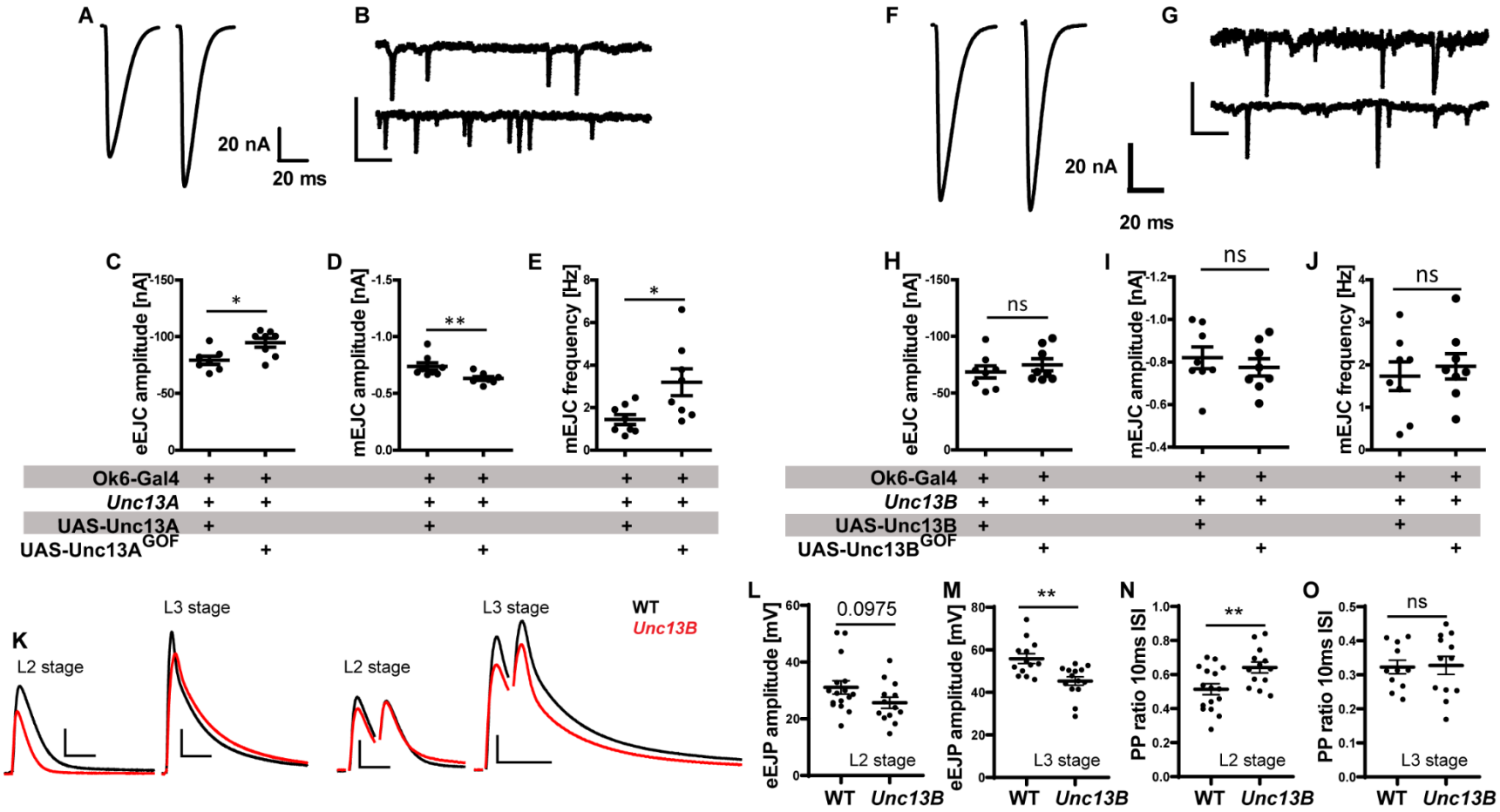

Figure S6. Gain-of-function mutation in Unc13A results in increased evoked and spontaneous release. Related to figure 5.

(A) Representative eEJC traces and (B) mEJC traces for motoneuron expression of Unc13A and Unc13A^{GOF} constructs in *Unc13A* mutants. (C) eEJC amplitudes are higher, (D) mEJC amplitudes are lower and (E) mEJC frequency is higher upon reexpression of Unc13A^{GOF} construct in *Unc13A* mutants compared to controls. (F) Representative eEJC traces and (G) Representative mEJC

traces for motoneuron expression of Unc13B and Unc13B^{GOF} constructs in *Unc13B* mutants. (H) eEJC amplitudes, (I) mEJC amplitudes and (J) mEJC frequency are all unchanged upon reexpression of Unc13B^{GOF} construct in *Unc13B* mutants compared to controls. (K) Representative traces of eEJP and paired-pulse (inter stimulus interval (ISI) of 10ms) measurements at larval muscle 6/7 NMJs of L2/L3 developmental stages. eEJP amplitudes are lower in *Unc13B* mutants at both (L) L2 and (M) L3 larval stages. PP ratio (10ms ISI) in *Unc13B* mutants is higher at (N) L2, but not (O) L3 developmental stage.